Int. J. Heat Mass Transfer. Vol. 30, No. 11, pp. 2319–2329, 1987
Printed in Great Britain

0017–9310/87 $3.00 + 0.00

Natural convection heat transfer in a square enclosure containing water near its density maximum

D. S. LIN and M. W. NANSTEEL
Department of Mechanical Engineering and Applied Mechanics, University of Pennsylvania, Philadelphia, PA 19104, U.S.A.

(*Received* 21 *October* 1985 *and in final form* 2 *April* 1987)

Abstract—The steady-state flow structure, temperature and heat transfer in a square enclosure heated and cooled on opposite vertical walls and containing cold water near its density maximum are investigated numerically. Interpretation of the results hinges upon a dimensionless density distribution parameter which fixes the orientation of the hot and cold wall temperatures with respect to the extremum temperature and also serves to characterize the distribution of the buoyancy force in the enclosure. Multicellular flow structures are observed for certain ranges of the density distribution parameter independent of the value of Rayleigh number ($10^3 \leqslant Ra \leqslant 10^6$). The effect of the density distribution parameter on cross-cavity heat transfer is found to be substantial and is discussed in the context of the changing flow structure. Comparisons with previous studies in the literature are made.

1. INTRODUCTION

THE MAJORITY of work in natural convection deals with fluids the densities of which monotonically increase or decrease linearly with temperature. However, for some fluids such as water and molten bismuth, antimony and gallium, the density–temperature relation exhibits an extremum. Because the coefficient of thermal expansion changes sign at this extremum, the linear relation $\rho = \rho_0[(1-\beta(\bar{T}-\bar{T}_0)]$ is inadequate for these fluids when the range of temperature under consideration is in the neighborhood of the density extremum. Among the anomalous liquids mentioned above, water is by far the most important because its density extremum occurs near 4°C at atmospheric pressure. A number of studies have investigated the effect of the density extremum for water in detail, however, a large proportion of the work relates to external boundary layer flow past vertical or horizontal walls. The convection of cold water (i.e. near 4°C) in enclosures has been addressed in several studies. Forbes and Cooper [1] carried out a numerical study of the transient cooling of water in a rectangular enclosure through 4°C from above. Vasseur and Robillard [2] investigated the transient cooling of water in a rectangular enclosure with vertical and horizontal walls maintained at 0°C. The same authors [3, 4] studied supercooling as well as the transient behavior of cold water in a rectangular enclosure with a constant rate of cooling at the boundary. Altimer [5] has examined the flow in a rectangular box filled with a cold water-saturated porous media while Nguyen *et al.* [6] considered the case of a horizontal annulus filled with cold water. Also, Lin and Nansteel [7] studied the case of cold water convection in a vertical annulus in which the effects of curvature are discussed in detail. A number of experimental and analytical studies have been carried out for the steady natural convection of water near 4°C in a rectangular enclosure with vertical walls maintained at two different temperatures while the horizontal walls are adiabatic. Watson [8] seems to have been the first to investigate natural convection in a differentially heated cavity filled with cold water. In ref. [8] it was found that the anomalous density–temperature relationship may result in a dual, counter-rotating cell flow pattern which significantly inhibits cross-cavity heat transfer. The effect of temperature-dependent viscosity was also addressed in ref. [8] and was found to result in changes in magnitude rather than the character of the flow. Nansteel *et al.* [9] studied the heat transfer and flow structure in a differentially heated rectangular enclosure containing cold water by a perturbation technique in the small Rayleigh number regime. The numerical study of Desai and Forbes [10] considered the natural convection of cold water in a rectangular enclosure in which one vertical wall was held at 0°C (or 2°C) while the opposing wall was maintained at 8°C (or 6°C). Aspect ratios of 1 and 3 were considered. Robillard and Vasseur [11] performed a numerical study of a cold water-filled square enclosure in which one vertical wall was kept at 0°C while the temperature of the other vertical wall was varied between 4 and 12°C. Thermal boundary conditions on the horizontal walls were either linear in temperature or adiabatic. Seki *et al.* [12] carried out experimental and numerical work on the same problem for an enclosure height of 100 mm. In ref. [12] aspect ratios of 1, 2, 5, 10 and 20 were considered. It was noted that aspect ratios near unity resulted in the maximum heat transfer. Recently,

NOMENCLATURE

c_p	constant pressure specific heat
g	gravitational acceleration
k	thermal conductivity
L	length of enclosure side
$Nu(x, y)$	local Nusselt number, equation (18)
$Nu(x)$	vertically averaged Nusselt number, equation (19)
$\bar{p}$	modified pressure, $\bar{p}' + \rho_c g \bar{y}$
$\bar{p}'$	pressure
Pr	Prandtl number, ν/α
q	exponent in density–temperature relation, equation (7)
q''	heat flux
R	density distribution parameter, $(\bar{T}_m - \bar{T}_c)/(\bar{T}_h - \bar{T}_c)$
Ra	Rayleigh number, $g\rho_m \alpha_1 L^3 (\bar{T}_h - \bar{T}_c)^q / \rho_c \nu \alpha$
$\bar{T}$	temperature
t	dimensionless time, $\bar{t}\nu/L^2$
$\bar{t}$	time
u	dimensionless horizontal velocity, $\bar{u}L/\nu$
$\bar{u}$	horizontal component of velocity
v	dimensionless vertical velocity, $\bar{v}L/\nu$
$\bar{v}$	vertical component of velocity
x	dimensionless horizontal coordinate, $\bar{x}/L$
$\bar{x}$	horizontal coordinate
y	dimensionless vertical coordinate, $\bar{y}/L$
$\bar{y}$	vertical coordinate.

Greek symbols

α	thermal diffusivity
α_1	constant in density–temperature relation, equation (7)
β	coefficient of thermal expansion
ν	kinematic viscosity
ξ	dimensionless vorticity, $\bar{\xi}L^2/\nu$
$\bar{\xi}$	vorticity
ρ	density
ϕ	dimensionless temperature, $(\bar{T} - \bar{T}_c)/(\bar{T}_h - \bar{T}_c)$
ψ	dimensionless streamfunction, $\bar{\psi}/\nu$
$\bar{\psi}$	streamfunction.

Subscripts

c	cold wall
h	hot wall
m	density extremum
0	reference state
1/2	vertical mid-plane of the enclosure.

Inaba and Fukuda [13, 14] investigated the effect of inclination angle on the natural convection of cold water in a rectangular enclosure both experimentally and numerically. In ref. [13] it was found that the two counter-rotating eddies are strongly influenced by the angle of inclination.

The present study addresses the steady convection of cold water in a square enclosure. The vertical walls are maintained at different temperatures while the horizontal boundaries are insulated. A non-dimensional parameter (similar to the one used first by Gebhart and Mollendorf [15] and later by Altimer [5] and Nguyen *et al.* [6]) is used to characterize the orientation of the vertical wall temperatures with respect to the extremum temperature. This parameter also characterizes the distribution of buoyancy forces in the enclosure and hence provides a very convenient and concise generalized framework for studying the effects of changing wall temperature. Numerical calculations are made to separately study the effects of Rayleigh number and buoyancy force distribution. The flow structure and temperature fields are discussed as well as the overall heat transfer.

2. MATHEMATICAL FORMULATION

The configuration considered here is that of a square enclosure of side length L. The vertical walls

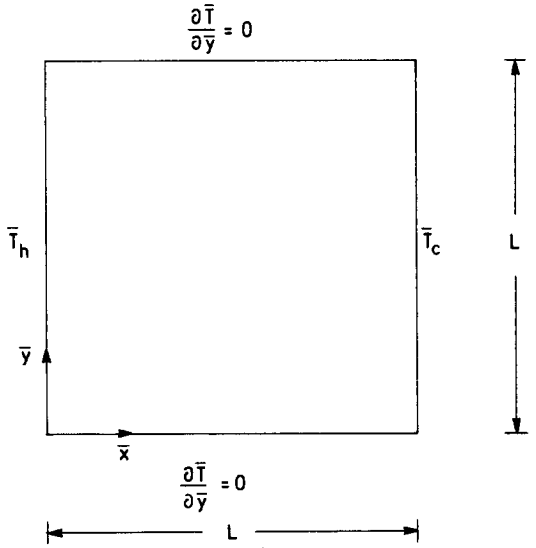

FIG. 1. Differentially heated square enclosure.

are maintained at temperatures $\bar{T}_h$ and $\bar{T}_c$ while the horizontal walls are insulated, Fig. 1. The enclosure is supposed sufficiently long in depth normal to the plane of Fig. 1 that the flow field is essentially the same in planes of different depth. The enclosed fluid is pure water and the temperature range of interest

is, $0°C \leqslant \bar{T}_c < \bar{T}_h \lesssim 20°C$, where density inversion phenomena are significant.

2.1. *Governing equations*

In formulating the governing equations the following assumptions are made:

(1) the flow is laminar and two-dimensional;

(2) physical properties, except for the density in the buoyancy force term, are constant and are evaluated at the cold wall temperature, $\bar{T}_c$;

(3) viscous dissipation is negligible.

With these assumptions, the governing equations, in their unsteady form, are

$$\frac{\partial \bar{u}}{\partial \bar{x}} + \frac{\partial \bar{v}}{\partial \bar{y}} = 0 \tag{1}$$

$$\frac{D\bar{u}}{D\bar{t}} = -\frac{1}{\rho_c}\frac{\partial \bar{p}'}{\partial \bar{x}} + \nu \nabla^2 \bar{u} \tag{2}$$

$$\frac{D\bar{v}}{D\bar{t}} = -\frac{1}{\rho_c}\frac{\partial \bar{p}'}{\partial \bar{y}} + \nu \nabla^2 \bar{v} - \frac{\rho}{\rho_c} g \tag{3}$$

$$\frac{D\bar{T}}{D\bar{t}} = \alpha \nabla^2 \bar{T}. \tag{4}$$

Defining the modified pressure, $\bar{p} = \bar{p}' + \rho_c g \bar{y}$, yields

$$\frac{\partial \bar{p}'}{\partial \bar{y}} = \frac{\partial \bar{p}}{\partial \bar{y}} - g\rho_c. \tag{5}$$

Initially, the fluid is assumed to be motionless and at the uniform temperature $(\bar{T}_h + \bar{T}_c)/2$. The corresponding initial and boundary conditions are

$$\begin{aligned}
&\bar{t} = 0: \\
&\bar{u} = \bar{v} = 0, \quad \bar{T} = \frac{\bar{T}_h + \bar{T}_c}{2} \\
&\bar{t} > 0: \\
&\bar{T}(0, \bar{y}) = \bar{T}_h, \quad \bar{T}(L, \bar{y}) = \bar{T}_c \\
&\frac{\partial \bar{T}}{\partial \bar{y}}(\bar{x}, 0) = \frac{\partial \bar{T}}{\partial \bar{y}}(\bar{x}, L) = 0 \\
&\bar{u} = \bar{v} = 0, \quad \text{on the boundary.}
\end{aligned} \tag{6}$$

Many correlations have been used to represent the density of cold water as a function of temperature, e.g. Kell [16], Chen and Millero [17] and Gebhart and Mollendorf [18]. Though most of these correlations are in close agreement, the correlation of Gebhart and Mollendorf is especially simple and very accurate. It has been widely used and will be adopted here because of its simple form. In ref. [18] the density of pure water at atmospheric pressure is given as

$$\rho = \rho_m [1 - \alpha_1 |\bar{T} - \bar{T}_m|^q] \tag{7}$$

where $\rho_m = 999.9720$ kg m^{-3}, $\alpha_1 = 9.297173 \times 10^{-6}$ $(°C)^{-q}$, $\bar{T}_m = 4.029325°C$ and $q = 1.894816$. In the range $0 \leqslant \bar{T} \leqslant 20°C$ this equation agrees with the very precise density relation of Kell [16] to within 6 p.p.m.

Introducing equations (5) and (7), equations (2) and (3) become

$$\frac{D\bar{u}}{D\bar{t}} = -\frac{1}{\rho_c}\frac{\partial \bar{p}}{\partial \bar{x}} + \nu \nabla^2 \bar{u} \tag{8}$$

$$\frac{D\bar{v}}{D\bar{t}} = -\frac{1}{\rho_c}\frac{\partial \bar{p}}{\partial \bar{y}} + \frac{g\alpha_1 \rho_m}{\rho_c}[|\bar{T} - \bar{T}_m|^q - |\bar{T}_c - \bar{T}_m|^q] + \nu \nabla^2 \bar{v}. \tag{9}$$

2.2. *Stream function–vorticity* $(\bar{\psi} - \bar{\xi})$ *formation*

The pressure is eliminated by cross-differentiating and combining equations (8) and (9). Also, the streamfunction $\bar{\psi}$ and vorticity $\bar{\xi}$ are defined as

$$\frac{\partial \bar{\psi}}{\partial \bar{y}} = \bar{u}, \quad \frac{\partial \bar{\psi}}{\partial \bar{x}} = -\bar{v}, \quad \bar{\xi} = -\nabla^2 \bar{\psi}. \tag{10}$$

Defining the non-dimensional variables

$$\begin{aligned}
&x = \frac{\bar{x}}{L}, \quad y = \frac{\bar{y}}{L} \\
&u = \frac{\bar{u}L}{\nu}, \quad v = \frac{\bar{v}L}{\nu}, \quad \phi = \frac{\bar{T} - \bar{T}_c}{\bar{T}_h - \bar{T}_c} \\
&\psi = \frac{\bar{\psi}}{\nu}, \quad \xi = \frac{\bar{\xi}L^2}{\nu}, \quad t = \frac{\bar{t}\nu}{L^2}
\end{aligned}$$

the governing equations in dimensionless form become

$$\frac{D\xi}{Dt} = \frac{Ra}{Pr} q |\phi - R|^{q-2}(\phi - R)\frac{\partial \phi}{\partial x} + \nabla^2 \xi \tag{11}$$

$$\frac{D\phi}{Dt} = \frac{1}{Pr}\nabla^2 \phi \tag{12}$$

$$\nabla^2 \psi = -\xi. \tag{13}$$

The initial and boundary conditions take the form

$$\begin{aligned}
&t = 0: \\
&u = v = 0, \quad \phi = 1/2 \\
&t > 0: \\
&\phi(0, y) = 1, \quad \phi(1, y) = 0 \\
&\frac{\partial \phi}{\partial y}(x, 0) = \frac{\partial \phi}{\partial y}(x, 1) = 0 \\
&\psi = \frac{\partial \psi}{\partial x} = \frac{\partial \psi}{\partial y} = 0, \quad \text{on the boundary.}
\end{aligned} \tag{14}$$

Additional dimensionless parameters appearing in equations (11) and (12) are the Rayleigh and Prandtl numbers

$$Ra = \frac{g\rho_m \alpha_1 L^3 (\bar{T}_h - \bar{T}_c)^q}{\rho_c \nu \alpha}, \quad Pr = \frac{\nu}{\alpha}$$

and the density distribution parameter

$$R = \frac{\bar{T}_m - \bar{T}_c}{\bar{T}_h - \bar{T}_c}. \tag{15}$$

This parameter will be seen to be very important due

to its fundamental effect on the flow field and heat transfer in the enclosure and is essentially equivalent to the 'inversion parameter' used by Nguyen *et al.* [6] in their horizontal annulus study. The density distribution parameter essentially fixes the orientation of the maximum density temperature $\bar{T}_m$ with respect to the vertical wall temperatures $\bar{T}_h$ and $\bar{T}_c$. As shown in ref. [9] the case $R < 0$ ($\bar{T}_h > \bar{T}_c > \bar{T}_m$) results in density increasing monotonically with x across the enclosure. This density distribution results in a clockwise recirculation pattern. When $R > 1$ ($\bar{T}_m > \bar{T}_h > \bar{T}_c$) the distribution is reversed and hence a counter-clockwise pattern results. When R is in the range $0 < R < 1$ the wall temperatures $\bar{T}_h$ and $\bar{T}_c$ straddle the maximum density temperature $\bar{T}_m$. In this case as x varies from 0 to 1 density increases to a maximum $\rho = \rho_m$ at $\bar{T} = \bar{T}_m$ and then decreases. As a result, maximum density fluid at temperature $\bar{T}_m$ lies between warm low density fluid near the hot wall and cool fluid, also of relatively low density near the cold wall. Hence this heavier fluid at $\bar{T} = \bar{T}_m$ in the enclosure interior descends while the lighter fluid adjacent to the vertical boundaries ascends, giving rise to a pair of counter-rotating vortices arranged horizontally in the enclosure. It will be seen later, however, that this two-cell structure may not occur for $R \lesssim 1$ and $R \gtrsim 0$ due to viscous effects.

The symmetry of the density equation (7) with respect to the extremum temperature suggests that ψ and ϕ may also be symmetric in some fashion. In fact it can be easily shown that the system, equations (11)–(14), exhibits the symmetry properties

$$\begin{aligned} \psi(x, y; R) &= -\psi(1-x, y; 1-R) \\ \phi(x, y, R) &= 1-\phi(1-x, y; 1-R). \end{aligned} \tag{16}$$

Hence the flow and temperature fields for the case $R = 1/2+\Delta R$ can be obtained from the case $R = 1/2-\Delta R$ using equations (16). In particular, for $R = 1/2$, equations (16) state that the flow structure is symmetric with respect to the vertical centerline of the enclosure, $x = 1/2$.

2.3. *Heat transfer*

The local heat flux in the horizontal direction in the enclosure can be expressed as the superposition of conductive and convective modes, i.e.

$$q'' = -k\frac{\partial \bar{T}}{\partial \bar{x}} + \rho_c c_p(\bar{T}-\bar{T}_c)\bar{u}. \tag{17}$$

In dimensionless form, this becomes

$$Nu(x, y) = \frac{q''L}{k(\bar{T}_h-\bar{T}_c)} = -\frac{\partial \phi}{\partial x} + Pr\,\phi u. \tag{18}$$

Then the Nusselt number averaged over a vertical cross-section is

$$Nu(x) = \int_0^1 Nu(x, y)\,dy. \tag{19}$$

3. NUMERICAL SOLUTION

Numerical results were obtained by solving equations (11)–(13) subject to the accompanying boundary and initial conditions (14) by a finite-difference method. A false-transient approach was used to obtain steady-state solutions. First-order forward differences were used to approximate time derivatives while central difference approximations were used for spatial derivatives. The resulting set of algebraic equations was solved by the alternating direction implicit (ADI) technique which yields a system of algebraic equations in tridiagonal form to which the Thomas algorithm [19] can be applied. The size of the time step which led to a stable calculation in the present work depended upon grid size, Rayleigh number and the initial conditions. The results for the lowest Rayleigh number considered ($Ra = 10^3$) were obtained from a rest initial condition ($\psi = \xi = u = v = 0$, $\phi = 1/2$). For higher values of Ra, the steady solution for a somewhat smaller Rayleigh number was used as the initial state. It is also noted that the steady-state solution was found to be independent of the choice of initial condition.

For each case (Ra, R) mesh refinement was continued until adequate pointwise convergence was observed in ψ, ξ and ϕ as well as convergence of global heat transfer. The mesh size required for satisfactory convergence was found to be strongly dependent on Ra, as shown in Table 1, for the case $R = 2/3$. In Table 1, Nu_h and Nu_c were obtained from equation

Table 1. Convergence of Nu and ψ with mesh size, $R = 2/3$

Ra	Mesh	Nu_h	$Nu_{1/2}$	Nu_c	ψ_{max}	ψ_{min}
10^3	21×21	1.018	1.019	1.018	0.0386	−0.00027
	21×21	1.600	1.618	1.603	0.260	−0.0037
10^4	31×31	1.601	1.612	1.609	0.260	−0.0036
	41×41	1.602	1.612	1.610	0.260	−0.0036
	21×21	3.323	3.356	3.326	0.698	−0.070
10^5	31×31	3.334	3.347	3.348	0.703	−0.067
	41×41	3.344	3.348	3.349	0.706	−0.065
	21×21	5.860	6.854	6.566	1.431	−0.778
10^6	31×31	6.554	6.546	6.513	1.372	−0.609
	41×41	6.560	6.525	6.552	1.386	−0.579
	61×61	6.561	6.534	6.560	1.390	−0.562

(19) with $x = 0$ and 1, respectively. For the case $R = 1/2$, advantage was taken of the symmetry property (16), so that calculations were necessary for one-half of the enclosure only. All results were obtained with $Pr = 13.0$.

4. RESULTS AND DISCUSSION

4.1. *Streamfunction and temperature*

The steady flow patterns which result for the square enclosure containing cold water are in general a consequence of the local balance between buoyancy, viscous and inertia forces. For small values of Ra, however, inertia effects are relatively unimportant so that an approximate balance between viscous and buoyancy forces results. Figure 2 shows the results for ψ at $Ra = 10^3$ for values of the density distribution parameter $R = 0.4$, 1/2, 0.55, 2/3 and 3/4. For $Ra = 10^3$ the temperature field deviates from the pure conduction field, $\phi = 1 - x$, only slightly due to convective effects. However, the perturbation on the pure conduction temperature field due to convection increases in magnitude with $|R - 1/2|$. In the case, $R = 1/2$, the hot and cold wall temperatures perfectly straddle $\bar{T}_m$. From the symmetry relations (16) the maximum density contour (coinciding with the temperature contour, $\phi_m = R = 1/2$) is located at the enclosure mid-plane $x = 1/2$. Dense fluid near $x = 1/2$ falls while less dense fluid adjacent to the hot and cold walls rises. This results in a symmetric pair of counter-rotating vortices in the left and right halves of the enclosure. As R increases (decreases) the maximum density contour moves toward the hot (cold) wall. As a result the counter-clockwise-rotating cell on the right in the case $R = 0.4$ becomes stronger and larger at the expense of the clockwise-rotating cell on the left as R increases. For $R = 2/3$ the cell on the left has divided into two separate clockwise-rotating cells in the upper and lower left-hand corners of the enclosure. In this case even though the maximum density contour ($\phi_m = 2/3$) is located approximately at $x = 1/3$, upflow on the hot wall occurs only near the corners of the enclosure. The circulation of the counter-clockwise right-hand vortex has become so strong that it drags (by virtue of the fluid's viscosity) relatively light fluid downward along the hot wall, overpowering the upward buoyancy force there. When $\phi_m = R = 3/4$, even the two corner cells are eliminated by the strong counter-clockwise-rotating cell on the right resulting in a completely unicellular flow. In the instance $R = 1$, density increases with temperature and hence decreases with x everywhere in the enclosure resulting in a single counter-clockwise-rotating cell.

Figure 3 shows the ψ and ϕ fields for $R = 1/2$ and $Ra = 10^4$ and 10^6. Note that the bicellular flow structure observed for $Ra = 10^3$, $R = 1/2$, Fig. 2, persists for $10^4 \leqslant Ra \leqslant 10^6$ with the cells becoming more angular in shape. Due to symmetry (16) the flow in the left and right halves of the enclosure is identical except for the sense of rotation. Notice, Fig. 3, $Ra = 10^6$, that the ϕ-field is developing boundary layer-like characteristics with increasing Ra near $x = 1/2$ as well as near the vertical walls. The large gradients in temperature near $x = 1/2$, $y \lesssim 1$, are due to the intense circulation of the two counter-rotating cells which deposits warm fluid from the hot wall and cool fluid from the cold wall in the top-center region of the enclosure.

In the case $R = 0.55$, Fig. 4, there is no spatial symmetry. The maximum density contour $\phi_m = R = 0.55$ has now shifted (from $x = 1/2$ for $R = 1/2$) toward the hot wall. With increasing Ra the larger counter-clockwise cell adjacent to the cold wall becomes more dominant. Cool fluid is swept across the upper boundary and into the upper left-hand corner of the enclosure. This shifts the maximum density contour $\phi_m = 0.55$ toward the hot wall in the upper half of the enclosure. As a result, for $Ra = 10^6$ there is no upflow along the upper portion of the hot wall because the strong counter-clockwise vortex overcomes the (upward) buoyancy force in the fluid directly adjacent to the upper portion of the hot wall. It will be seen later that this direct contact of the cooler fluid with the upper section of the hot wall substantially increases heat transfer across the enclosure above the symmetrical, $R = 1/2$, case. Note also that at higher values of Rayleigh number ($Ra = 10^6$) the structure of the flow and temperature fields to the right of the maximum density contour, $\phi_m = 0.55$, are developing some characteristics which are observed in the convection of Boussinesq fluids at large Ra. For example it is observed, Fig. 4, $Ra = 10^6$, that fluid in the large counter-clockwise cell exhibits an increasing degree of density stratification with increasing Ra. Note, however, that here, warm fluid underlies cooler fluid since density is increasing with temperature for $\phi < \phi_m = 0.55$. The basic structure of the flow field for $R = 2/3$ exhibited the same features as the case $R = 0.55$ with the left-hand clockwise-rotating cell confined to a smaller region in the lower left-hand corner of the enclosure. For $R = 2/3$ the small cell in the upper left-hand corner at $Ra = 10^3$ (Fig. 2) does not appear for $10^4 \leqslant Ra \leqslant 10^6$. For $R = 0.75$ the flow consists of a single counter-clockwise vortex for $Ra = 10^3$, Fig. 2, while for $10^4 \leqslant Ra \leqslant 10^6$ the flow structure is similar to the case $R = 2/3$, i.e. a weak clockwise rotating cell is observed in the lower left-hand corner of the enclosure.

4.2. *Heat transfer*

Table 2 lists the vertically averaged Nusselt number (19) for six values of R in the range $0.4 \leqslant R \leqslant 1$ and $Ra = 10^3$, 10^4, 10^5 and 10^6. Due to the symmetry in the temperature field (16) heat transfer is symmetric with respect to $R = 1/2$, hence $Nu(R = 0) = Nu(R = 1)$, $Nu(R = 1/3) = Nu(R = 2/3)$, etc. Figure 5 shows the variation of Nu with R for fixed Ra. The most striking feature of this figure is the

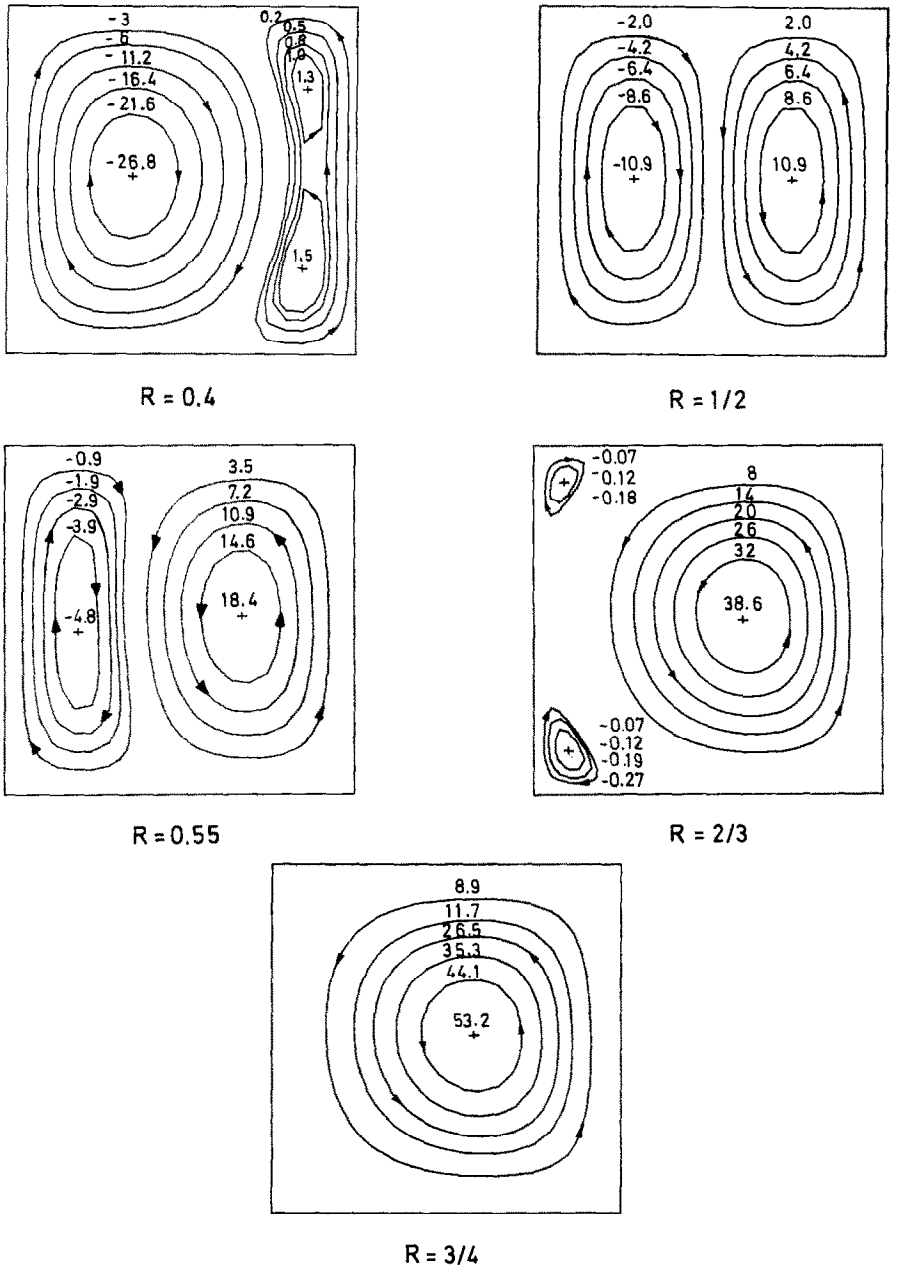

FIG. 2. Streamfunction ($\psi \times 10^3$) contours for $Ra = 10^3$.

minimum in heat transfer at $R = 1/2$. This minimum has also been observed in previous works, however, typically, the variation of Nu with increasing $\bar{T}_h$ is examined for fixed $\bar{T}_c$. When Nu is displayed in this manner both R and Ra are varying. In Fig. 5 the effect of the density distribution parameter is clearly displayed without introducing additional Rayleigh number effects. The minimum at $R = 1/2$ in Fig. 5 is due to the symmetric, dual-cell flow structure which results when $\bar{T}_h$ and $\bar{T}_c$ straddle the maximum density temperature $\bar{T}_m$. The dual-cell structure prohibits direct convective transfer between the hot and cold walls. Each cell behaves like an insulator preventing warm (cool) fluid from the hot (cold) wall from coming in contact with the cold (hot) wall. The only direct thermal communication between the two walls occurs near $x = 1/2$, where the warm and cool streams meet and energy is transferred primarily by conduction. Heat transfer increases very sharply for R-values away from $R = 1/2$ when Ra is large because then one of the two cells in the enclosure wets both walls (see Fig. 4, $Ra = 10^6$). Figure 6 shows the variation of Nu with Ra for various values of R. For large Ra the heat transfer behavior is similar to that observed for a Boussinesq fluid, that is

$$Nu \propto Ra^{0.29}$$

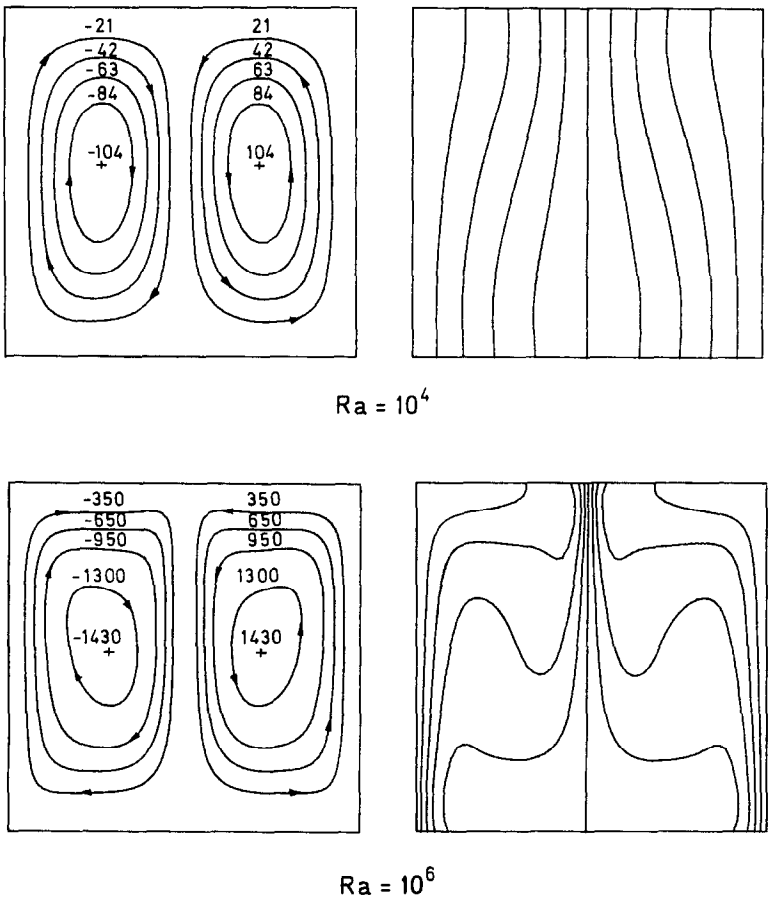

FIG. 3. Streamfunction ($\psi \times 10^3$) and temperature ($\phi = 0(0.1)1$) contours for $R = 1/2$.

independent of R. The behavior for large Ra is seen to blend smoothly into the conduction dominated regime, $Nu \sim 1$, for smaller Ra.

4.3. *Comparison with previous work*

In earlier work on cold water enclosure convection, heat transfer results are often presented with the cold wall temperature $\bar{T}_c$ held fixed while $\bar{T}_h$ is varied. If this is done both Ra and R are varying parameters. For completeness the results of the present calculation are plotted in this way, Fig. 7, along with the constant viscosity results of Watson [8] and the variable property results of Inaba and Fukuda [13]. In ref. [8] calculations of Nu were obtained for a square enclosure with $\bar{T}_c = 0°C$, $Pr = 13.7$ and

$$\frac{g|\beta_c|L^3}{\nu\alpha} = 10^3\,K^{-1}$$

while in ref. [13] $\bar{T}_c = 0°C$, $gL^3/\nu_c^2 = 1.02 \times 10^7$ and $Pr = 13$. Note that the present results are in good agreement with both refs. [8, 13] for $\bar{T}_h \lesssim 8°C$, beyond which both refs. [8, 13] yield lower estimates of the heat transfer. In the case of Watson's results, one factor which may contribute to this discrepancy is the density–temperature relation used. The relation due to Watson differs from the very accurate $\rho - \bar{T}$ relation of Kell [16] by as much as 26 p.p.m. while equation (7) is accurate to within less than 6 p.p.m. in the range 0–20°C. Recall that the density difference between 0 and 4°C (and hence the sole driving force for convection) is only about 130 p.p.m. Also, the value of β_c used is critical. In the comparison with ref. [8], at each value of $\bar{T}_h$ the present value of Ra is calculated as

$$Ra = \frac{\rho_m \alpha_1 \bar{T}_h^q}{\rho_c|\beta_c|} \times 10^3 = 136.64\bar{T}_h^q \qquad (20)$$

where the property value $\beta_c = -6.805 \times 10^{-5}\,K^{-1}$ has been used [20]. The value of β_c given by Watson's ρ–$\bar{T}$ relation is $-8.94 \times 10^{-5}\,K^{-1}$ which is about 30% larger. The value given by equation (7) is $\beta_c = -6.1 \times 10^{-5}\,K^{-1}$. Using a larger value of β_c in equation (20) would result in a smaller value of Ra and hence smaller values of Nu for the present calculation in the comparison of Fig. 7. The discrepancy observed between the present results and the results of Inaba and Fukuda [13] might also be due, in part, to differences in the ρ–$\bar{T}$ relation used. However, it is also likely that differences are present due to property (ν, k) variations with temperature which are accounted for by Inaba and Fukuda but are not accounted for in the present study. Also, some of the

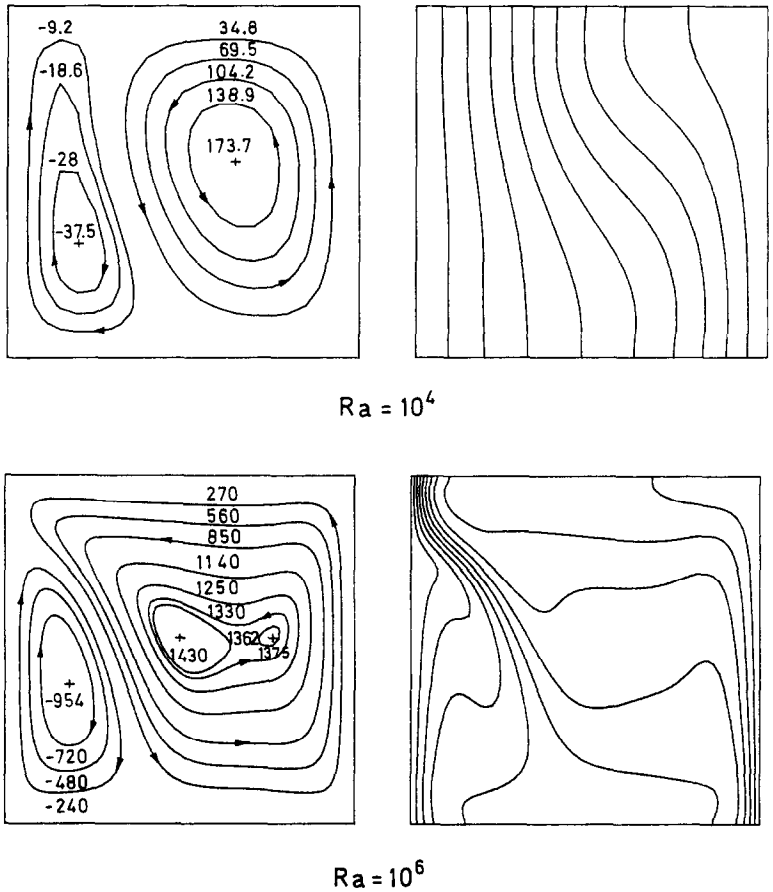

FIG. 4. Streamfunction ($\psi \times 10^3$) and temperature ($\phi = 0(0.1)1$) contours for $R = 0.55$.

Table 2. Nusselt number variation with R and Ra

	R					
Ra	0.4	1/2	0.55	2/3	3/4	1
10^3	1.007	1.0009	1.002	1.018	1.038	1.119
10^4	1.391	1.076	1.202	1.608	1.834	2.278
10^5	2.853	2.080	2.416	3.347	3.823	4.709
10^6	5.685	4.090	4.860	6.560	7.445	9.195

discrepancy may be due to discretization error in the calculation of ref. [13]. Inaba and Fukuda use a 21×21 finite difference grid and upwind differencing to make computations for Ra as large as 3.5×10^5. Note, from Table 1 that at $Ra = 10^6$ a 21×21 mesh is quite inadequate to resolve Nu even when employing the more accurate central difference approximation. Figure 8 shows the horizontal temperature profile at the enclosure midheight for $R = 1/2$ and $Ra = 6.3 \times 10^4$ for ref. [13] and the present study. Note that the results of ref. [13] show a quite mild horizontal temperature gradient near the center of the enclosure, $x \simeq 1/2$, while the present results suggest that a thermal boundary layer is beginning to form where the two symmetrical counter-rotating rolls meet (see also Fig. 3). The profile due to ref. [13] appears to have much the same shape as one would expect in a unicellular Boussinesq case, that is, most of the temperature change occurs near the heated and cooled walls. For reasons which are not clear the temperature profile of ref. [13] gives very little evidence of the dual-cell structure even though the results of ref. [13] for ψ agree quite well with the present findings.

5. CONCLUSIONS

The flow structure, temperature field and heat transfer in a square enclosure containing cold water have been calculated numerically. A parameter, R, introduced through scaling of the governing equations, was used to fix the orientation of the hot and cold wall temperatures with respect to the extre-

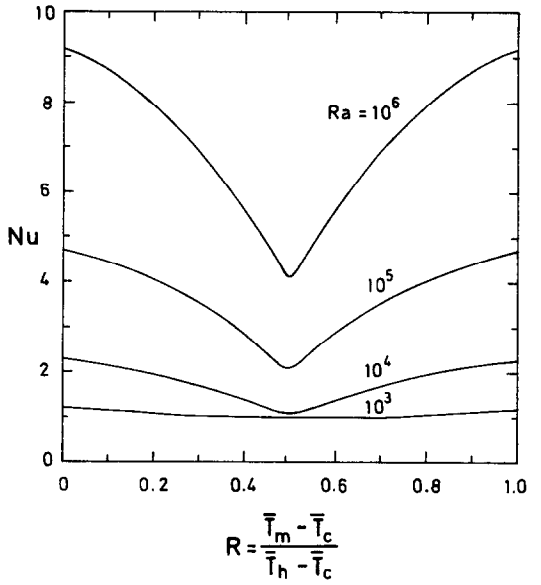

FIG. 5. Heat transfer variation with R.

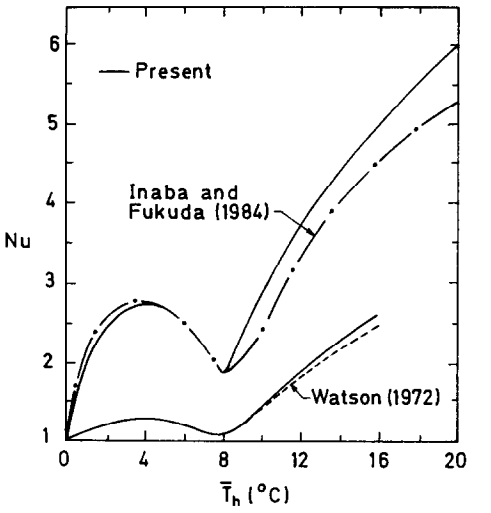

FIG. 7. Heat transfer variation with $\bar{T}_h$, $\bar{T}_c = 0°C$: ---, Watson [8], $g|\beta_c|L^3/\nu_c\alpha_c = 10^3 K^{-1}$, $Pr = 13.7$; -·-, Inaba and Fukuda [13], $gL^3/\nu_c^2 = 1.02 \times 10^7$, $Pr = 13$; ——, present.

mum temperature. This parameter was also found to be convenient for characterizing the distribution of density and hence the buoyancy force distribution in the enclosure. For $0 < R < 1$ the relationship between fluid density and temperature in the enclosure has an extremum and hence regions of the flow field exhibit buoyancy force reversals which under some circumstances result in multicellular flows. The flow was shown to be symmetric (in the sense of equations (16)) with respect to the density distribution parameter value $R = 1/2$. The effects of R ($0 \leqslant R \leqslant 1$) and Rayleigh number ($10^3 \leqslant Ra \leqslant 10^6$) on the flow and heat transfer were examined separately. It was found that while R determines, to a large extent, the number and sense of circulation of the cells in the flow, Rayleigh number affects, for the most part, only the cell shapes and locations within the enclosure. Boundary layer effects were noted for large values of Ra. A rather pronounced minimum in cross-cavity heat transfer was observed for $R = 1/2$ in which case the hot and cold wall temperatures straddle the extremum temperature. The resulting symmetrical, counter-rotating, dual-cell flow structure greatly inhibits convective transfer between the heated and cooled walls. Comparisons with previous cold water studies indicated good agreement in the heat transfer only for $R \lesssim 1/2$.

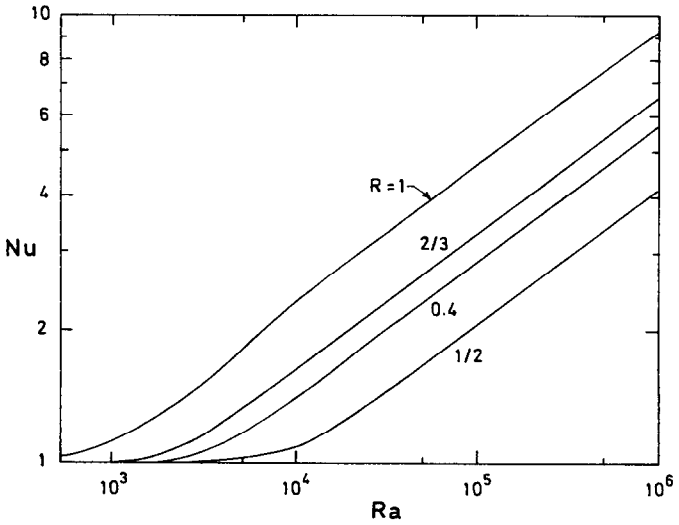

FIG. 6. Heat transfer variation with Ra.

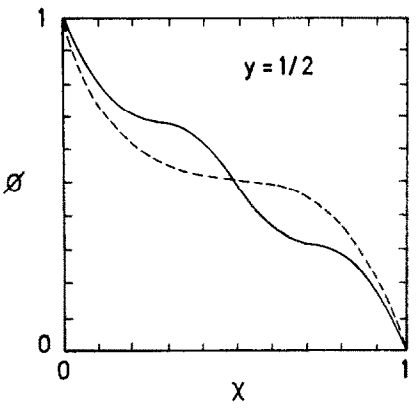

FIG. 8. Horizontal temperature profile at $y = 1/2$, $\bar{T}_h = 8°C$, $\bar{T}_c = 0°C$: ---, Inaba and Fukuda [13], $gL^3/\nu_c^2 = 1.02 \times 10^7$, $Pr = 13$; ——, present.

Substantial differences from the present results were found in the temperature field behavior predicted in ref. [13].

Acknowledgement—The authors wish to thank the National Science Foundation for its support under grant number MEA 84-14322. The authors also wish to acknowledge the helpful comments of Professor B. Gebhart and Ms E. Mitchell for her efficient preparation of the manuscript.

REFERENCES

1. R. E. Forbes and J. W. Cooper, Natural convection in a horizontal layer of water cooled from above to near freezing, *J. Heat Transfer* **97,** 47–53 (1975).
2. P. Vasseur and L. Robillard, Transient natural convection heat transfer in a mass of water cooled through 4°C, *Int. J. Heat Mass Transfer* **23,** 1195–1205 (1980).
3. L. Robillard and P. Vasseur, Transient natural convection heat transfer of water with maximum density effect and supercooling, *J. Heat Transfer* **103,** 528–534 (1981).
4. L. Robillard and P. Vasseur, Convective response of a mass of water near 4°C to a constant cooling rate applied on its boundaries, *J. Fluid Mech.* **118,** 123–141 (1982).
5. I. Altimer, Convection naturelle tridimensionnelle en milieu poreux satur par un fluide presentant un maximum de densité, *Int. J. Heat Mass Transfer* **27,** 813–824 (1984).
6. T. H. Nguyen, P. Vasseur and L. Robillard, Natural convection between horizontal concentric cylinders with density inversion of water for low Rayleigh numbers, *Int. J. Heat Mass Transfer* **25,** 1559–1568 (1982).
7. D. S. Lin and M. W. Nansteel, Natural convection in a vertical annulus containing water near the density maximum, *J. Heat Transfer* (1987), in press.
8. A. Watson, The effect of the inversion temperature on the convection of water in an enclosed rectangular cavity, *Q. J. Mech. Appl. Math.* **25,** 423–446 (1972).
9. M. W. Nansteel, K. Medjani and D. S. Lin, Natural convection of water near its density maximum in a rectangular enclosure: low Rayleigh number calculations, *Physics Fluids* **30**(2), 312–317 (1987).
10. V. S. Desai and R. E. Forbes, Free convection in water in the vicinity of maximum density, *Envir. Geophys. Heat Transfer* 41–47 (1971).
11. L. Robillard and P. Vasseur, Effet du maximum de densité sur la convection libre de l'eau dans une cavité fermée, *Can. J. Civil Engng* **6**(4), 481–493 (1979).
12. N. Seki, S. Fukusako and H. Inaba, Free convective heat transfer with density inversion in a confined rectangular vessel, *Wärme- und Stoffübertragung* **11,** 145–156 (1978).
13. H. Inaba and T. Fukuda, Natural convection in an inclined square cavity in regions of density inversion of water, *J. Fluid Mech.* **142,** 363–381 (1984).
14. H. Inaba and T. Fukuda, An experimental study of natural convection in an inclined rectangular cavity filled with water at its density extremum, *J. Heat Transfer* **106,** 109–115 (1984).
15. B. Gebhart and J. C. Mollendorf, Buoyancy-induced flows in water under conditions in which density extrema may arise, *J. Fluid Mech.* **89,** 673–707 (1978).
16. G. S. Kell, Precise representation of volume properties of water at one atmosphere, *J. Chem. Engng Data* **12,** 66–69 (1967).
17. C. T. Chen and F. J. Millero, The specific volume of sea water at high pressures, *Deep Sea Res.* **23,** 595–612 (1976).
18. B. Gebhart and J. C. Mollendorf, A new density relation for pure and saline water, *Deep Sea Res.* **24,** 831–848 (1977).
19. A. S. Householder, *The Theory of Matrices in Numerical Analysis*. Blaisdell, New York (1964).
20. *CRC Handbook of Chemistry and Physics*. Chemical Rubber Company, Cleveland, Ohio (1981).

CONVECTION THERMIQUE NATURELLE DANS UNE CAVITE CARREE CONTENANT DE L'EAU PRES DE SON MAXIMUM DE DENSITE

Résumé—On étudie numériquement la structure de l'écoulement permanent, la température et le transfert thermique dans une cavité carrée chauffée et refroidie sur les parois verticales opposées et qui contient de l'eau froide proche de son maximum de densité. L'interprétation des résultats repose sur un paramètre adimensionnel de distribution de densité qui fixe l'orientation des températures des parois chaude et froide par rapport à l'extrémum de température et qui sert aussi à caractériser la distribution de la force de flottement dans la cavité. Les structures multicellulaires sont observées pour certains domaines du paramètre de distribution de densité indépendamment de la valeur du nombre de Rayleigh ($10^3 \leqslant Ra \leqslant 10^6$). L'effet du paramètre de distribution de densité sur le transfert à travers la cavité est très sensible et on le discute relativement aux changements de structure de l'écoulement. Des comparaisons sont faites avec les études antérieures.

WÄRMEÜBERTRAGUNG DURCH NATÜRLICHE KONVEKTION IN EINEM QUADRATISCHEN GEFÄSS, DAS WASSER IM BEREICH DES DICHTEMAXIMUMS ENTHÄLT

Zusammenfassung—Die stationären Strömungsstrukturen, die Temperaturverteilung und die Wärmeübertragung in einem quadratischen Gefäß, das auf zwei gegenüberliegenden Seiten beheizt bzw. gekühlt wird und kaltes Wasser im Bereich des Dichtemaximums enthält, werden numerisch untersucht. Die Auswertung der Ergebnisse konzentriert sich auf den dimensionslosen 'Dichteverteilungs-Parameter', der die Lage der Temperaturen an der heißen bzw. kalten Wand in Bezug auf die Extremtemperatur festlegt und außerdem die Auftriebsverteilung im Behälter beschreibt. Für bestimmte Bereiche des Dichteverteilungs-Parameters werden unabhängig von den Werten der Rayleigh-Zahl ($10^3 \leqslant Ra \leqslant 10^6$) multizellulare Strömungsstrukturen beobachtet. Es wurde festgestellt, daß der Einfluß des Dichteverteilungs-Parameters auf die Wärmeübertragung im Gefäß von grundsätzlicher Bedeutung ist; dieser Einfluß wird im Zusammenhang mit der sich ändernden Strömungsstruktur diskutiert. Es wurden Vergleiche mit Untersuchungen angestellt, welche in der Literatur beschrieben sind.

СВОБОДНОКОНВЕКТИВНЫЙ ТЕПЛОПЕРЕНОС В ПОЛОСТИ КВАДРАТНОГО СЕЧЕНИЯ, ЗАПОЛНЕННОЙ ВОДОЙ, ПЛОТНОСТЬ КОТОРОЙ БЛИЗКА К МАКСИМАЛЬНОЙ

Аннотация—Численно исследуются стационарные структура течения, температурное поле и теплоперенос в нагреваемой и охлаждаемой вдоль вертикальных противоположных стенок полости квадратного сечения, заполненной холодной водой, плотность которой близка к максимальной. В качестве режимного параметра для интерпретации результатов выбран безразмерный параметр распределения плотности, характеризующий отличие температур холодной и горячей стенок от экстремальной температуры, а также распределение подъемной силы в полости. В определенном диапазоне изменения параметра распределения плотности, не зависящем от величины числа Рэлея ($10^3 \leq Ra \leq 10^6$), наблюдаются многоячеистые структуры течения. Обнаружена отчетливая зависимость теплопереноса поперек полости от величины параметра распределения плотности. Обсуждается изменение этой зависимости при изменении структуры течения. Проведено сравнение полученных результатов с аналогичными опубликованными в литературе данными.